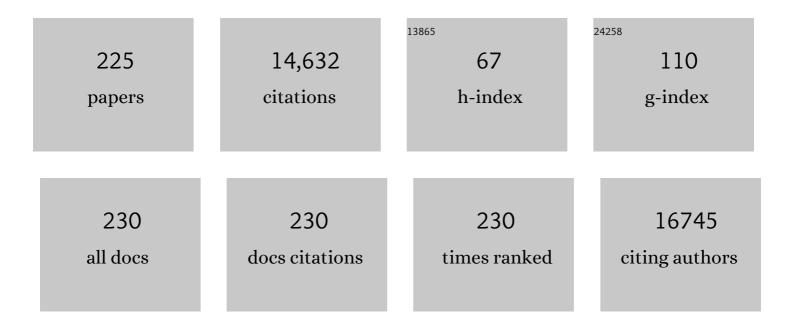
## Hexing Li

List of Publications by Year in descending order

Source: https://exaly.com/author-pdf/4099491/publications.pdf Version: 2024-02-01



HEVING LI

#	Article	IF	CITATIONS
1	Photoelectrocatalytic Reduction of CO <sub>2</sub> to Syngas via SnO <i><sub>x</sub></i> â€Enhanced Cu <sub>2</sub> O Nanowires Photocathodes. Advanced Functional Materials, 2022, 32, 2109600.	14.9	42
2	Blue Energy for Green Hydrogen Fuel: A Selfâ€Powered Electrochemical Conversion System Driven by Triboelectric Nanogenerators. Advanced Energy Materials, 2022, 12, .	19.5	52
3	Fully biodegradable water-soluble triboelectric nanogenerator for human physiological monitoring. Nano Energy, 2022, 93, 106787.	16.0	55
4	Microwaveâ€Positioning Assembly: Structure and Surface Optimizations for Catalysts. Small Structures, 2022, 3, .	12.0	6
5	Microwave one-pot synthesis of CNT-supported amorphous Ni–P alloy nanoparticles with enhanced hydrogenation performance. Journal of Materials Chemistry A, 2022, 10, 6560-6568.	10.3	10
6	Potassium as a Versatile Promoter to Tailor the Distribution of the Olefins in CO <sub>2</sub> Hydrogenation over Ironâ€Based Catalyst. ChemCatChem, 2022, 14, .	3.7	10
7	CO2 conversion via dry reforming of methane on a core-shell Ru@SiO2 catalyst. Journal of CO2 Utilization, 2022, 57, 101893.	6.8	18
8	Polarization field promoted photoelectrocatalysis for synergistic environmental remediation and H2 production. Chemical Engineering Journal, 2022, 437, 135132.	12.7	20
9	Systematic Assessment of Precious Metal Recovery to Improve Environmental and Resource Protection. ACS ES&T Engineering, 2022, 2, 1039-1052.	7.6	22
10	Carbon Nanotube-Threaded Mesocrystalline CeO <sub>2</sub> for Enhanced Photocatalytic NO Removal. ACS Applied Nano Materials, 2022, 5, 3581-3590.	5.0	12
11	Aqueous Photocatalytic Recycling of Gold and Palladium from Waste Electronics and Catalysts. ACS ES&T Engineering, 2022, 2, 1445-1453.	7.6	11
12	The Fluorineâ€Rich Electrolyte as an Interface Modifier to Stabilize Lithium Metal Battery at Ultra‣ow Temperature. Advanced Functional Materials, 2022, 32, .	14.9	38
13	Photoelectrocatalytic sterilization on thorn-like ZIF-67/ZnO hybrid photoanodes. Journal of Environmental Chemical Engineering, 2022, 10, 107385.	6.7	8
14	Bimetallic CoxCuy-CAT-1 metal-organic frameworks for synergistic antibacterial contribution of photocatalytic-photothermal effect. Journal of Environmental Chemical Engineering, 2022, 10, 107582.	6.7	6
15	Singlet Oxygen and Mobile Hydroxyl Radicals Co-operating on Gas–Solid Catalytic Reaction Interfaces for Deeply Oxidizing NO <sub><i>x</i></sub> . Environmental Science & Technology, 2022, 56, 5830-5839.	10.0	22
16	Challenges of photocatalysis and their coping strategies. Chem Catalysis, 2022, 2, 1315-1345.	6.1	83
17	Rutile TiO2 nanorods grown on carbon nanotubes as high-performance lithium-ion batteries anode via one-dimensional electron pathways. Journal of Sol-Gel Science and Technology, 2022, 103, 437-446.	2.4	3
18	A novel ternary MQDs/NCDs/TiO <sub>2</sub> nanocomposite that collaborates with activated persulfate for efficient RhB degradation under visible light irradiation. New Journal of Chemistry, 2021, 45, 1327-1338.	2.8	17

#	Article	IF	CITATIONS
19	Dual electrocatalytic heterostructures for efficient immobilization and conversion of polysulfides in Li–S batteries. Journal of Materials Chemistry A, 2021, 9, 18477-18487.	10.3	15
20	Electrospun Polymer Nanofibers with TiO <sub>2</sub> @NiCo-LDH as Efficient Polysulfide Barriers for Wide-Temperature-Range Li–S Batteries. ACS Applied Materials & Interfaces, 2021, 13, 2734-2744.	8.0	37
21	Improved Degradation Efficiency of Levofloxacin by a Self-Powered Electrochemical System with Pulsed Direct-Current. ACS Nano, 2021, 15, 5478-5485.	14.6	25
22	Selective recovery of precious metals through photocatalysis. Nature Sustainability, 2021, 4, 618-626.	23.7	188
23	Efficient photocatalytic hydrogen peroxide generation coupled with selective benzylamine oxidation over defective ZrS3 nanobelts. Nature Communications, 2021, 12, 2039.	12.8	90
24	Controlling the Gas–Water Interface to Enhance Photocatalytic Degradation of Volatile Organic Compounds. ACS ES&T Engineering, 2021, 1, 1140-1148.	7.6	23
25	Power Management and Reaction Optimization for a Self-Powered Electrochemical System Driven by a Triboelectric Nanogenerator. Nano Letters, 2021, 21, 5633-5640.	9.1	22
26	One-pot synthesis of 3D porous Bi7O9I3/N-doped graphene aerogel with enhanced photocatalytic activity for organic dye degradation in wastewater. Ceramics International, 2021, 47, 19556-19566.	4.8	17
27	<i>In Situ</i> Synthesis of a Li <sub>6.4</sub> La <sub>3</sub> Zr <sub>1.4</sub> Ta <sub>0.6</sub> O <sub>12</sub> /Poly(vinylene) Tj ETQq Energy Materials, 2021, 4, 9368-9375.	1 1.0.784	-314.rgBT /0
28	1T and 2H mixed phase MoS2 nanobelts coupled with Ti3+ self-doped TiO2 nanosheets for enhanced photocatalytic degradation of RhB under visible light. Applied Surface Science, 2021, 556, 149768.	6.1	38
29	Pressure-dependent band-bending in ZnO: A near-ambient-pressure X-ray photoelectron spectroscopy study. Journal of Energy Chemistry, 2021, 60, 25-31.	12.9	3
30	Heterostructuring Mesoporous 2D Iridium Nanosheets with Amorphous Nickel Boron Oxide Layers to Improve Electrolytic Water Splitting. Small Methods, 2021, 5, e2100679.	8.6	40
31	A novel amorphous alloy photocatalyst (NiB/In2O3) composite for sunlight-induced CO2 hydrogenation to HCOOH. Applied Catalysis B: Environmental, 2021, 298, 120603.	20.2	49
32	Self-Driven Reactive Oxygen Species Generation via Interfacial Oxygen Vacancies on Carbon-Coated TiO <sub>2–<i>x</i></sub> with Versatile Applications. ACS Applied Materials & Interfaces, 2021, 13, 2033-2043.	8.0	34
33	Precious metal recovery. Joule, 2021, 5, 3097-3115.	24.0	79
34	Divergent Synthesis of Contorted Polycyclic Aromatics Containing Pentagons, Heptagon, and/or Azulene. Organic Letters, 2021, , .	4.6	8
35	Long-Life and High-Rate-Charging Lithium Metal Batteries Enabled by a Flexible Active Solid Electrolyte Interphase Layer. ACS Applied Materials & Interfaces, 2021, 13, 60678-60688.	8.0	9
36	Novel S-doped ordered mesoporous carbon nanospheres toward advanced lithium metal anodes. Nano Energy, 2020, 69, 104443.	16.0	52

#	Article	IF	CITATIONS
37	A mesoporous non-precious metal boride system: synthesis of mesoporous cobalt boride by strictly controlled chemical reduction. Chemical Science, 2020, 11, 791-796.	7.4	58
38	Cooperation between inside and outside of TiO2: Lattice Cu+ accelerates carrier migration to the surface of metal copper for photocatalytic CO2 reduction. Applied Catalysis B: Environmental, 2020, 264, 118515.	20.2	93
39	Primary amine-functionalized mesoporous phenolic resin as an effective and stable solid base catalyst for Knoevenagel reactions in water. Green Synthesis and Catalysis, 2020, 1, 79-82.	6.8	14
40	Efficient Self-Driving Photoelectrocatalytic Reactor for Synergistic Water Purification and H <sub>2</sub> Evolution. ACS Applied Materials & Interfaces, 2020, 12, 44731-44742.	8.0	33
41	A strong hydrangea-like Au–TiO <sub>2</sub> catalyst for round-the-clock degradation of oxalic acid in the presence of ozone. Catalysis Science and Technology, 2020, 10, 7481-7485.	4.1	5
42	Polarity- and Pressure-Dependent Hydrogen Dynamics on ZnO Polar Surfaces Revealed by Near-Ambient-Pressure X-ray Photoelectron Spectroscopy. Journal of Physical Chemistry C, 2020, 124, 25431-25436.	3.1	4
43	Cumulene Wires Display Increasing Conductance with Increasing Length. Nano Letters, 2020, 20, 8415-8419.	9.1	47
44	Photoelectrocatalytic bacterial inactivation of <i>Acinetobacter baumannii</i> on Cu <sub>2</sub> O/TiO <sub>2</sub> @Cu mesh photoanodes. Catalysis Science and Technology, 2020, 10, 7378-7385.	4.1	9
45	Visible light-catalytic hydroxylation of aryl halides with water to phenols by carbon nitride and nickel complex cooperative catalysis. Green Chemistry, 2020, 22, 7417-7423.	9.0	32
46	Amorphous Alloy Architectures in Pore Walls: Mesoporous Amorphous NiCoB Alloy Spheres with Controlled Compositions <i>via</i> a Chemical Reduction. ACS Nano, 2020, 14, 17224-17232.	14.6	46
47	Self-Suspended Photothermal Microreactor for Water Desalination and Integrated Volatile Organic Compound Removal. ACS Applied Materials & Interfaces, 2020, 12, 51537-51545.	8.0	47
48	Stringing the Perylene Diimide Bow. Angewandte Chemie - International Edition, 2020, 59, 14303-14307.	13.8	23
49	Ordered Mesoporous Ni–P Amorphous Alloy Nanowire Arrays: High-Efficiency Catalyst for Production of Polyol from Sugar. ACS Applied Materials & Interfaces, 2020, 12, 26101-26112.	8.0	25
50	MOFs Conferred with Transient Metal Centers for Enhanced Photocatalytic Activity. Angewandte Chemie, 2020, 132, 17335-17339.	2.0	11
51	MOFs Conferred with Transient Metal Centers for Enhanced Photocatalytic Activity. Angewandte Chemie - International Edition, 2020, 59, 17182-17186.	13.8	121
52	Selective CO <sub>2</sub> reduction to HCOOH on a Pt/In <sub>2</sub> O <sub>3</sub> /g-C <sub>3</sub> N <sub>4</sub> multifunctional visible-photocatalyst. RSC Advances, 2020, 10, 22460-22467.	3.6	15
53	Stringing the Perylene Diimide Bow. Angewandte Chemie, 2020, 132, 14409-14413.	2.0	5
54	Multi-functional anodes boost the transient power and durability of proton exchange membrane fuel cells. Nature Communications, 2020, 11, 1191.	12.8	65

#	Article	IF	CITATIONS
55	In Situ One-Step Synthesis of Platinum Nanoparticles Supported on Metal–Organic Frameworks as an Effective and Stable Catalyst for Selective Hydrogenation of 5-Hydroxymethylfurfural. ACS Omega, 2020, 5, 16183-16188.	3.5	13
56	Solid-Phase Microwave Reduction of WO <sub>3</sub> by GO for Enhanced Synergistic Photo-Fenton Catalytic Degradation of Bisphenol A. ACS Applied Materials & amp; Interfaces, 2020, 12, 32604-32614.	8.0	41
57	NH2-UiO-66(Zr) with fast electron transfer routes for breaking down nitric oxide via photocatalysis. Applied Catalysis B: Environmental, 2020, 267, 118687.	20.2	83
58	Mesoporous Metal–Metalloid Amorphous Alloys: The First Synthesis of Open 3D Mesoporous Niâ€B Amorphous Alloy Spheres via a Dual Chemical Reduction Method. Small, 2020, 16, e1906707.	10.0	37
59	An efficient defect engineering strategy to enhance catalytic performances of Co3O4 nanorods for CO oxidation. Journal of Hazardous Materials, 2020, 394, 122540.	12.4	43
60	Gas-Phase Photoelectrocatalytic Oxidation of NO <i>via</i> TiO <sub>2</sub> Nanorod Array/FTO Photoanodes. Environmental Science & Technology, 2020, 54, 5902-5912.	10.0	42
61	Magnetically induced synthesis of mesoporous amorphous CoB nanochains for efficient selective hydrogenation of cinnamaldehyde to cinnamyl alcohol. Chemical Engineering Journal, 2020, 398, 125564.	12.7	33
62	Microwave-induced Assembly of CuS@MoS <sub>2</sub> Core-shell Nanotubes and Study on Their Photocatalytic Fenton-like Reactions. Acta Chimica Sinica, 2020, 78, 961.	1.4	12
63	A novel visible-light-driven ternary Ag@Ag <sub>2</sub> O/BiOCl Z-scheme photocatalyst with enhanced removal efficiency of RhB. New Journal of Chemistry, 2019, 43, 13929-13937.	2.8	25
64	Controlling Singlet Fission by Molecular Contortion. Journal of the American Chemical Society, 2019, 141, 13143-13147.	13.7	47
65	Strong Hollow Spherical La <sub>2</sub> NiO <sub>4</sub> Photocatalytic Microreactor for Round-the-Clock Environmental Remediation. ACS Applied Materials & Interfaces, 2019, 11, 25967-25975.	8.0	33
66	Edgeâ€Enriched Ultrathin MoS <sub>2</sub> Embedded Yolkâ€6hell TiO <sub>2</sub> with Boosted Charge Transfer for Superior Photocatalytic H <sub>2</sub> Evolution. Advanced Functional Materials, 2019, 29, 1901958.	14.9	115
67	Dual-Stimulus Smart Actuator and Robot Hand Based on a Vapor-Responsive PDMS Film and Triboelectric Nanogenerator. ACS Applied Materials & Interfaces, 2019, 11, 42504-42511.	8.0	31
68	Hybrid Cu <sub>2</sub> O/TiO <sub>2</sub> Nanocomposites with Enhanced Photocatalytic Antibacterial Activity toward <i>Acinetobacter Baumannii</i> . ACS Applied Bio Materials, 2019, 2, 4892-4903.	4.6	29
69	Self-powered electrochemical system by combining Fenton reaction and active chlorine generation for organic contaminant treatment. Nano Research, 2019, 12, 2729-2735.	10.4	35
70	Directing isomerization reactions of cumulenes with electric fields. Nature Communications, 2019, 10, 4482.	12.8	97
71	Surfactant Pyrolysis-Guided in Situ Fabrication of Primary Amine-Rich Ordered Mesoporous Phenolic Resin Displaying Efficient Heavy Metal Removal. ACS Applied Materials & Interfaces, 2019, 11, 21815-21821.	8.0	22
72	Lithiophilic CuO Nanoflowers on Tiâ€Mesh Inducing Lithium Lateral Plating Enabling Stable Lithiumâ€Metal Anodes with Ultrahigh Rates and Ultralong Cycle Life. Advanced Energy Materials, 2019, 9, 1900853.	19.5	103

#	Article	IF	CITATIONS
73	Woodâ€Derived Materials for Advanced Electrochemical Energy Storage Devices. Advanced Functional Materials, 2019, 29, 1902255.	14.9	157
74	Photocatalysis: Microwaveâ€Induced Metal Dissolution Synthesis of Core–Shell Copper Nanowires/ZnS for Visible Light Photocatalytic H <sub>2</sub> Evolution (Adv. Energy Mater. 22/2019). Advanced Energy Materials, 2019, 9, 1970085.	19.5	2
75	Gas-Phase Photoelectrocatalysis for Breaking Down Nitric Oxide. Environmental Science & Technology, 2019, 53, 7145-7154.	10.0	45
76	Microwaveâ€Induced Metal Dissolution Synthesis of Core–Shell Copper Nanowires/ZnS for Visible Light Photocatalytic H <sub>2</sub> Evolution. Advanced Energy Materials, 2019, 9, 1900775.	19.5	97
77	Self-driven photodetection based on impedance matching effect between a triboelectric nanogenerator and a MoS2 nanosheets photodetector. Nano Energy, 2019, 59, 492-499.	16.0	50
78	A chloroplast structured photocatalyst enabled by microwave synthesis. Nature Communications, 2019, 10, 1570.	12.8	88
79	Controlled Assembly of Hierarchical Metal Catalysts with Enhanced Performances. CheM, 2019, 5, 805-837.	11.7	24
80	Synthesis, Regioselective Bromination, and Functionalization of Coronene Tetracarboxydiimide. Journal of Organic Chemistry, 2019, 84, 2713-2720.	3.2	14
81	Efficient Photocatalytic Fuel Cell via Simultaneous Visible-Photoelectrocatalytic Degradation and Electricity Generation on a Porous Coral-like WO <sub>3</sub> /W Photoelectrode. Environmental Science & Technology, 2019, 53, 3697-3706.	10.0	105
82	Mesoporous PtCu Alloy Nanoparticles with Tunable Compositions and Particles Sizes Using Diblock Copolymer Micelle Templates. Chemistry - A European Journal, 2019, 25, 343-348.	3.3	29
83	Photocatalytic Composite of a Floating BiOBr@Graphene Oxide@Melamine Foam for Efficient Removal of Organics. ChemCatChem, 2018, 10, 2394-2400.	3.7	16
84	Aerosol-Assisted Rapid Fabrication of a Heterogeneous Organopalladium Catalyst with Hierarchical Bimodal Pores. ACS Applied Materials & Interfaces, 2018, 10, 13914-13923.	8.0	8
85	Microwave irradiation induced UIO-66-NH2 anchored on graphene with high activity for photocatalytic reduction of CO2. Applied Catalysis B: Environmental, 2018, 228, 47-53.	20.2	186
86	CO <sub>2</sub> conversion to synthesis gas <i>via</i> DRM on the durable Al <sub>2</sub> O <sub>3</sub> /Ni/Al <sub>2</sub> O <sub>3</sub> sandwich catalyst with high activity and stability. Green Chemistry, 2018, 20, 2781-2787.	9.0	43
87	In Situ High-Level Nitrogen Doping into Carbon Nanospheres and Boosting of Capacitive Charge Storage in Both Anode and Cathode for a High-Energy 4.5 V Full-Carbon Lithium-Ion Capacitor. Nano Letters, 2018, 18, 3368-3376.	9.1	163
88	Synergistic Ag/TiO2-N photocatalytic system and its enhanced antibacterial activity towards Acinetobacter baumannii. Applied Catalysis B: Environmental, 2018, 224, 175-182.	20.2	95
89	Synergistic Photocatalytic-Photothermal Contribution to Antibacterial Activity in BiOl-Graphene Oxide Nanocomposites. ACS Applied Bio Materials, 2018, 1, 2141-2152.	4.6	23
90	Unveiling the Role of Defects on Oxygen Activation and Photodegradation of Organic Pollutants. Environmental Science & Technology, 2018, 52, 13879-13886.	10.0	167

#	Article	IF	CITATIONS
91	Nanotube Array-Like WO <sub>3</sub> Photoanode with Dual-Layer Oxygen-Evolution Cocatalysts for Photoelectrocatalytic Overall Water Splitting. ACS Applied Energy Materials, 2018, 1, 6871-6880.	5.1	60
92	Aerosol-Assisted Synthesis of Spherical Sb/C Composites as Advanced Anodes for Lithium Ion and Sodium Ion Batteries. ACS Applied Energy Materials, 2018, 1, 6381-6387.	5.1	32
93	Recent Progress of Hybrid Solidâ€State Electrolytes for Lithium Batteries. Chemistry - A European Journal, 2018, 24, 18293-18306.	3.3	127
94	Bimetal MOF derived mesocrystal ZnCo2O4 on rGO with High performance in visible-light photocatalytic NO oxidization. Applied Catalysis B: Environmental, 2018, 236, 304-313.	20.2	128
95	Inflammation-free and gas-permeable on-skin triboelectric nanogenerator using soluble nanofibers. Nano Energy, 2018, 51, 260-269.	16.0	46
96	Enhanced Photocatalytic Degradation Performance by Fluid-Induced Piezoelectric Field. Environmental Science & Technology, 2018, 52, 7842-7848.	10.0	186
97	A facile approach for the synthesis of Z-scheme photocatalyst ZIF-8/g-C <sub>3</sub> N <sub>4</sub> with highly enhanced photocatalytic activity under simulated sunlight. New Journal of Chemistry, 2018, 42, 12180-12187.	2.8	66
98	Comprehensive suppression of single-molecule conductance using destructive σ-interference. Nature, 2018, 558, 415-419.	27.8	256
99	Graphyne-oxide supported Pd catalyst with ten times higher nitrobenzenes reduction activity than Pd/C. Research on Chemical Intermediates, 2018, 44, 6327-6337.	2.7	4
100	Graphyne-like Porous Carbon-rich Network Supported Pd Nanoparticles as an Efficient Catalyst for Suzuki-Miyaura Couplings under Aerobic Conditions. Current Nanoscience, 2018, 14, 503-510.	1.2	1
101	Photoelectrocatalytic reduction of CO 2 to methanol over a photosystem II-enhanced Cu foam/Si-nanowire system. Journal of Environmental Sciences, 2017, 60, 108-113.	6.1	19
102	Coupling system of Ag/BiOBr photocatalysis and direct contact membrane distillation for complete purification of N-containing dye wastewater. Chemical Engineering Journal, 2017, 317, 386-393.	12.7	78
103	Self-powered modulation of elastomeric optical grating by using triboelectric nanogenerator. Nano Energy, 2017, 38, 91-100.	16.0	80
104	Selfâ€Powered Electrostatic Actuation Systems for Manipulating the Movement of both Microfluid and Solid Objects by Using Triboelectric Nanogenerator. Advanced Functional Materials, 2017, 27, 1606408.	14.9	90
105	Pt-Enhanced Mesoporous Ti <sup>3+</sup> /TiO <sub>2</sub> with Rapid Bulk to Surface Electron Transfer for Photocatalytic Hydrogen Evolution. ACS Applied Materials & Interfaces, 2017, 9, 16959-16966.	8.0	147
106	A facile solvothermal approach for the synthesis of novel W-doped TiO <sub>2</sub> nanoparticles/reduced graphene oxide composites with enhanced photodegradation performance under visible light irradiation. New Journal of Chemistry, 2017, 41, 13382-13390.	2.8	22
107	Enhanced photoreduction of Cr( <scp>vi</scp> ) and photooxidation of NO over TiO <sub>2â^'x</sub> mesoporous single crystals. RSC Advances, 2017, 7, 55927-55934.	3.6	9
108	Self-Powered Electrostatic Filter with Enhanced Photocatalytic Degradation of Formaldehyde Based on Built-in Triboelectric Nanogenerators. ACS Nano, 2017, 11, 12411-12418.	14.6	169

#	Article	lF	CITATIONS
109	Dynamic kinetic resolution of aromatic <i>sec</i> -alcohols by using a heterogeneous palladium racemization catalyst and lipase. Catalysis Science and Technology, 2017, 7, 5838-5842.	4.1	16
110	A facile solvothermal approach of novel Bi2S3/TiO2/RGO composites with excellent visible light degradation activity for methylene blue. Applied Surface Science, 2017, 396, 58-66.	6.1	81
111	Hollow spherical RuO 2 @TiO 2 @Pt bifunctional photocatalyst for coupled H 2 production and pollutant degradation. Applied Catalysis B: Environmental, 2016, 194, 42-49.	20.2	130
112	Reduced Graphene Oxide-Immobilized Tris(bipyridine)ruthenium(II) Complex for Efficient Visible-Light-Driven Reductive Dehalogenation Reaction. ACS Applied Materials & Interfaces, 2016, 8, 12141-12148.	8.0	33
113	Macrocyclization in the Design of Organic n-Type Electronic Materials. Journal of the American Chemical Society, 2016, 138, 12861-12867.	13.7	101
114	A convenient approach of MIP/Co–TiO <sub>2</sub> nanocomposites with highly enhanced photocatalytic activity and selectivity under visible light irradiation. RSC Advances, 2016, 6, 69326-69333.	3.6	23
115	Porous CuO nanotubes/graphene with sandwich architecture as high-performance anodes for lithium-ion batteries. Nanoscale, 2016, 8, 19343-19351.	5.6	48
116	Solvothermal alcoholysis synthesis of hierarchical TiO 2 with enhanced activity in environmental and energy photocatalysis. Journal of Photochemistry and Photobiology C: Photochemistry Reviews, 2016, 28, 72-86.	11.6	84
117	Nanotube-confinement induced size-controllable g-C3N4 quantum dots modified single-crystalline TiO2 nanotube arrays for stable synergetic photoelectrocatalysis. Nano Energy, 2016, 19, 446-454.	16.0	329
118	BiOBr/Bi2MoO6 composite in flower-like microspheres with enhanced photocatalytic activity under visible-light irradiation. RSC Advances, 2016, 6, 13498-13504.	3.6	25
119	Synthesis of Mo-doped TiO <sub>2</sub> nanowires/reduced graphene oxide composites with enhanced photodegradation performance under visible light irradiation. RSC Advances, 2016, 6, 23809-23815.	3.6	23
120	Microwave-antenna induced in situ synthesis of Cu nanowire threaded ZIF-8 with enhanced catalytic activity in H <sub>2</sub> production. Nanoscale, 2016, 8, 7749-7754.	5.6	32
121	CNTs threaded (001) exposed TiO <sub>2</sub> with high activity in photocatalytic NO oxidation. Nanoscale, 2016, 8, 2899-2907.	5.6	50
122	Asymmetric Hydrosilylation of Aromatic Ketones Catalyzed by an Economical and Effective Copperâ€Diphosphine Catalytic System in Air. Chinese Journal of Chemistry, 2015, 33, 578-582.	4.9	10
123	A Hybridized Power Panel to Simultaneously Generate Electricity from Sunlight, Raindrops, and Wind around the Clock. Advanced Energy Materials, 2015, 5, 1501152.	19.5	174
124	BiOBr visible-light photocatalytic films in a rotating disk reactor for the degradation of organics. Journal of Materials Chemistry A, 2015, 3, 14801-14808.	10.3	32
125	Microwave-assisted synthesis of Ag-doped MOFs-like organotitanium polymer with high activity in visible-light driven photocatalytic NO oxidization. Applied Catalysis B: Environmental, 2015, 172-173, 46-51.	20.2	98
126	Plant Uptake-Assisted Round-the-Clock Photocatalysis for Complete Purification of Aquaculture Wastewater Using Sunlight. Environmental Science & Technology, 2015, 49, 2418-2424.	10.0	69

#	Article	IF	CITATIONS
127	Uniform anatase single-crystal cubes with high thermal stability fully enclosed by active {010} and {001} facets. RSC Advances, 2015, 5, 11029-11035.	3.6	12
128	Plasmonic silver quantum dots coupled with hierarchical TiO2 nanotube arrays photoelectrodes for efficient visible-light photoelectrocatalytic hydrogen evolution. Scientific Reports, 2015, 5, 10461.	3.3	113
129	Synthesis of Ce ions doped metal–organic framework for promoting catalytic H <sub>2</sub> production from ammonia borane under visible light irradiation. Journal of Materials Chemistry A, 2015, 3, 14134-14141.	10.3	102
130	Chiral Conjugated Corrals. Journal of the American Chemical Society, 2015, 137, 9982-9987.	13.7	104
131	Copper Nanowires: A Substitute for Noble Metals to Enhance Photocatalytic H <sub>2</sub> Generation. Nano Letters, 2015, 15, 4853-4858.	9.1	111
132	Hydrothermal synthesis of graphene/Fe <sup>3+</sup> -doped TiO <sub>2</sub> nanowire composites with highly enhanced photocatalytic activity under visible light irradiation. Journal of Materials Chemistry A, 2015, 3, 15214-15224.	10.3	64
133	A functionalized graphene oxide and nano-zeolitic imidazolate framework composite as a highly active and reusable catalyst for [3 + 3] formal cycloaddition reactions. Journal of Materials Chemistry A, 2015, 3, 14779-14785.	10.3	23
134	Enhancing Sorption Capacities for Copper(II) and Lead(II) under Weakly Acidic Conditions by <scp>l</scp> -Tryptophan-Functionalized Graphene Oxide. Journal of Chemical & Engineering Data, 2015, 60, 1469-1475.	1.9	49
135	Biochemical composite synthesized by stepwise crosslinking: An efficient platform for one-pot biomass conversion. Journal of Catalysis, 2015, 327, 78-85.	6.2	10
136	Exploring the Important Role of Nanocrystals Orientation in TiO <sub>2</sub> Superstructure on Photocatalytic Performances. Langmuir, 2015, 31, 3494-3499.	3.5	47
137	Highly Efficient and Stable Au/CeO <sub>2</sub> –TiO <sub>2</sub> Photocatalyst for Nitric Oxide Abatement: Potential Application in Flue Gas Treatment. Langmuir, 2015, 31, 10822-10830.	3.5	69
138	Hierarchical Nanostructured WO <sub>3</sub> with Biomimetic Proton Channels and Mixed Ionic-Electronic Conductivity for Electrochemical Energy Storage. Nano Letters, 2015, 15, 6802-6808.	9.1	157
139	Ag/BiOBr Film in a Rotating-Disk Reactor Containing Long-Afterglow Phosphor for Round-the-Clock Photocatalysis. ACS Applied Materials & Interfaces, 2015, 7, 20076-20082.	8.0	55
140	Ionothermal synthesis of black Ti <sup>3+</sup> -doped single-crystal TiO <sub>2</sub> as an active photocatalyst for pollutant degradation and H <sub>2</sub> generation. Journal of Materials Chemistry A, 2015, 3, 3748-3756.	10.3	141
141	Ru–B amorphous alloy deposited on mesoporous silica nanospheres: An efficient catalyst for d-glucose hydrogenation to d-sorbitol. Catalysis Today, 2015, 258, 327-336.	4.4	33
142	Plasmon-induced photoelectrocatalytic activity of Au nanoparticles enhanced TiO2 nanotube arrays electrodes for environmental remediation. Applied Catalysis B: Environmental, 2015, 164, 217-224.	20.2	182
143	Water-medium organic synthesis over active and reusable organometal catalysts with tunable nanostructures. Chemical Science, 2014, 5, 3695-3707.	7.4	19
144	Highly active, durable and recyclable ordered mesoporous magnetic organometallic catalysts for promoting organic reactions in water. Journal of Materials Chemistry A, 2014, 2, 484-491.	10.3	36

#	Article	IF	CITATIONS
145	Yolk–Shell Nanoarchitectures with a Ru-Containing Core and a Radially Oriented Mesoporous Silica Shell: Facile Synthesis and Application for One-Pot Biomass Conversion by Combining with Enzyme. ACS Applied Materials & Interfaces, 2014, 6, 20851-20859.	8.0	22
146	Amine-Functionalized GO as an Active and Reusable Acid–Base Bifunctional Catalyst for One-Pot Cascade Reactions. ACS Catalysis, 2014, 4, 394-401.	11.2	154
147	Supercritical solvothermal preparation of a Zn <sub>x</sub> Cd <sub>1â^'x</sub> S visible photocatalyst with enhanced activity. Journal of Materials Chemistry A, 2014, 2, 19641-19647.	10.3	44
148	Combination of Enzyme and Ru–B Amorphous Alloy Encapsulated in Yolk-Shell Silica for One-Pot Dextrin Conversion to Sorbitol. ACS Catalysis, 2014, 4, 251-258.	11.2	24
149	Dye-sensitized solar cells with enhanced efficiency using hierarchical TiO2spheres as a scattering layer. RSC Advances, 2014, 4, 36206.	3.6	12
150	<i>In Situ </i> Preparation of Au‣H@SO <sub>3</sub> H‣BAâ€15 Catalyst with Enhanced Activity and Durability in Alkyne Hydration. Chinese Journal of Chemistry, 2014, 32, 1072-1076.	4.9	8
151	Magnetically recoverable nanoparticles as efficient catalysts for organic transformations in aqueous medium. Green Chemistry, 2014, 16, 3401-3427.	9.0	232
152	Highly active, water-compatible and easily separable magnetic mesoporous Lewis acid catalyst for the Mukaiyama–Aldol reaction in water. Green Chemistry, 2014, 16, 3768-3777.	9.0	17
153	Au nanoparticles enhanced rutile TiO2 nanorod bundles with high visible-light photocatalytic performance for NO oxidation. Applied Catalysis B: Environmental, 2014, 147, 610-616.	20.2	119
154	Thin-Layer Polymer Wrapped Enzymes Encapsulated in Hierarchically Mesoporous Silica with High Activity and Enhanced Stability. Scientific Reports, 2014, 4, 4421.	3.3	13
155	Imidazoliumâ€Based Organic–Inorganic Hybrid Silica as a Functional Platform Dramatically Boosts Chiral Organometallics Performance in Asymmetric Catalysis. ChemCatChem, 2013, 5, 1784-1789.	3.7	23
156	An extremely stable and highly active periodic mesoporous Lewis acid catalyst in water-medium Mukaiyama-aldol reaction. Green Chemistry, 2013, 15, 2865.	9.0	15
157	Periodic mesoporous silicaâ€supported Ni(II) organometallic complex as an active and reusable nanocatalyst for waterâ€medium Sonogashira coupling reaction. Applied Organometallic Chemistry, 2013, 27, 512-518.	3.5	8
158	Preparation and visible light catalytic activity of three-dimensional ordered macroporous CdS/TiO2 films. Chinese Journal of Catalysis, 2013, 34, 949-955.	14.0	13
159	C <sub>60</sub> /Bi <sub>2</sub> TiO <sub>4</sub> F <sub>2</sub> Heterojunction Photocatalysts with Enhanced Visible-Light Activity for Environmental Remediation. ACS Applied Materials & Interfaces, 2013, 5, 7190-7197.	8.0	72
160	Ordered mesoporous TiO <sub>2</sub> with exposed (001) facets and enhanced activity in photocatalytic selective oxidation of alcohols. Journal of Materials Chemistry A, 2013, 1, 1296-1302.	10.3	90
161	Palladium nanoparticles encapsulated in porous silica shells: an efficient and highly stable catalyst for CO oxidation. RSC Advances, 2013, 3, 851-858.	3.6	38
162	Photoelectrocatalytic degradation of organic pollutants via a CdS quantum dots enhanced TiO2 nanotube array electrode under visible light irradiation. Nanoscale, 2013, 5, 2118.	5.6	205

#	Article	IF	CITATIONS
163	Supersized contorted aromatics. Chemical Science, 2013, 4, 2018.	7.4	141
164	Piperazine-functionalized ordered mesoporous polymer as highly active and reusable organocatalyst for water-medium organic synthesis. Green Chemistry, 2013, 15, 1665.	9.0	22
165	Synthesis of Ru-B amorphous alloy supported on SBA-15 with excellent catalytic efficiency in maltose hydrogenation. Chinese Journal of Catalysis, 2013, 34, 1027-1032.	14.0	16
166	An efficient round-the-clock La2NiO4 catalyst for breaking down phenolic pollutants. RSC Advances, 2012, 2, 4822.	3.6	25
167	Highly active and reusable organometallic catalysts covalently bonded to an ordered mesoporous polymer. Chemical Science, 2012, 3, 476-484.	7.4	28
168	Facile Synthesis of Co–B Amorphous Alloy in Uniform Spherical Nanoparticles with Enhanced Catalytic Properties. ACS Catalysis, 2012, 2, 2119-2125.	11.2	78
169	WO3 nanocrystals with tunable percentage of (001)-facet exposure. Applied Catalysis B: Environmental, 2012, 123-124, 398-404.	20.2	76
170	Suzuki Reactions in Water Catalyzed by an Active and Reusable PMOâ€Type Pd(II) Organometal Catalyst with Cageâ€Like Mesoporous Structure. Chinese Journal of Chemistry, 2012, 30, 2151-2157.	4.9	3
171	An Ionâ€Pair Immobilization Strategy in Rhodiumâ€Catalyzed Asymmetric Transfer Hydrogenation of Aromatic Ketones. Advanced Synthesis and Catalysis, 2012, 354, 3250-3258.	4.3	32
172	Enantioselective Addition of Malonates and βâ€Keto Esters to Nitroalkenes over an Organonickelâ€Functionalized Periodic Mesoporous Organosilica. Advanced Synthesis and Catalysis, 2012, 354, 3265-3274.	4.3	37
173	Sunlight-driven photodegradation of organic pollutants catalyzed by TiO2/(ZnS)x(CuInS2)1â^'x nanocomposites. Journal of Materials Chemistry, 2012, 22, 8759.	6.7	25
174	Ordered Mesoporous Proline Organocatalyst with High Activity and Strong Durability in Promoting Intermolecular Crossâ€Conjugated Additions. European Journal of Organic Chemistry, 2012, 2012, 3753-3758.	2.4	7
175	Comparative study on the mechanism in photocatalytic degradation of different-type organic dyes on SnS2 and CdS. Applied Catalysis B: Environmental, 2012, 123-124, 174-181.	20.2	219
176	Hollow Pt-Ni alloy nanospheres with tunable chamber structure and enhanced activity. Journal of Materials Chemistry, 2011, 21, 18447.	6.7	32
177	Active and reusable Pd( <scp>ii</scp> ) organometallic catalyst covalently bonded to mesoporous silica nanospheres for water-medium organic reactions. Chemical Science, 2011, 2, 961-966.	7.4	45
178	Influence of the Pd(II) Coordination Model on the Catalytic Performance of Pd–PPh <sub>2</sub> –SBA-15 in C–C Bond Forming Reactions. Journal of Physical Chemistry C, 2011, 115, 22514-22522.	3.1	19
179	Aerosolâ€Spraying Synthesis of Periodic Mesoporous Organometalsilica Spheres with Chamber Cavities as Active and Reusable Catalysts in Aqueous Organic Reactions. Advanced Functional Materials, 2011, 21, 3189-3197.	14.9	29
180	Magnetically Recoverable Nanoparticles: Highly Efficient Catalysts for Asymmetric Transfer Hydrogenation of Aromatic Ketones in Aqueous Medium. Advanced Synthesis and Catalysis, 2011, 353, 1317-1324.	4.3	44

Hexing Li

#	Article	IF	CITATIONS
181	A Novel Indiumâ€Boron Amorphous Alloy Mediator for Barbierâ€Type Carbonyl Allylation in Aqueous Medium. Advanced Synthesis and Catalysis, 2011, 353, 2131-2136.	4.3	16
182	Highly active and durable Bi2O3/TiO2 visible photocatalyst in flower-like spheres with surface-enriched Bi2O3 quantum dots. Applied Catalysis B: Environmental, 2011, 102, 120-125.	20.2	122
183	Synthesis of Hollow Gold Nanospheres and Their Applications in Surface-enhanced Raman Scattering and DNA Biosensor. Chinese Journal of Chemistry, 2010, 28, 2015-2019.	4.9	3
184	Solvothermally controllable synthesis of anatase TiO2 nanocrystals with dominant {001} facets and enhanced photocatalytic activity. CrystEngComm, 2010, 12, 2219.	2.6	178
185	Mesoporous silica-supported iridium catalysts for asymmetric hydrogenation reactions. Journal of Materials Chemistry, 2010, 20, 1970.	6.7	48
186	Hollow palladium–cobalt bimetallic nanospheres as an efficient and reusable catalyst for Sonogashira-type reactions. Journal of Materials Chemistry, 2010, 20, 4366.	6.7	38
187	Mesoporous Ni–B amorphous alloy microspheres with tunable chamber structure and enhanced hydrogenation activity. Chemical Communications, 2010, 46, 791-793.	4.1	48
188	Mesoporous Co–B amorphous alloy films with enhanced catalytic efficiency prepared from a mixed-surfactant solution. Journal of Materials Research, 2009, 24, 3300-3307.	2.6	8
189	Ultrasound-assisted synthesis of monodisperse Ru–B amorphous alloys with enhanced catalytic activity in maltose hydrogenation. Research on Chemical Intermediates, 2009, 35, 779-790.	2.7	14
190	Preparation of Mn2O3 catalyst with core–shell structure via spray pyrolysis assisted with glucose. Research on Chemical Intermediates, 2009, 35, 791-798.	2.7	11
191	Highly active TiO2â^'xâ^'yNxFy visible photocatalyst prepared under supercritical conditions in NH4F/EtOH fluid. Applied Catalysis B: Environmental, 2009, 89, 543-550.	20.2	101
192	Water-Medium Clean Organic Reactions over an Active Mesoporous Ru(II) Organometallic Catalyst. Environmental Science & Technology, 2009, 43, 188-194.	10.0	31
193	Microwave-assisted tandem allylation-isomerization reaction catalyzed by a mesostructured bifunctional catalyst in aqueous media. Green Chemistry, 2009, 11, 1477.	9.0	19
194	Hierarchical Assembly of Organic/Inorganic Building Molecules with <i>π</i> – <i>π</i> Interactions. Advanced Functional Materials, 2008, 18, 1526-1535.	14.9	29
195	Mesoporous Silica with Multiple Catalytic Functionalities. Advanced Functional Materials, 2008, 18, 3590-3597.	14.9	27
196	Vesicleâ€Assisted Assembly of Mesoporous Ceâ€Doped Pd Nanospheres with a Hollow Chamber and Enhanced Catalytic Efficiency. Advanced Functional Materials, 2008, 18, 3235-3241.	14.9	89
197	A Novel Rutheniumâ€Phosphorus Amorphous Alloy Catalyst for Maltose Hydrogenation to Maltitol. Advanced Synthesis and Catalysis, 2008, 350, 829-836.	4.3	26
198	Enantioselective Hydrogenation of Aromatic Ketones Catalyzed by a Mesoporous Silicaâ€Supported Iridium Catalyst. Advanced Synthesis and Catalysis, 2008, 350, 1464-1468.	4.3	36

#	Article	IF	CITATIONS
199	Highly Active TiO <sub>2-</sub> <i><sub>x</sub></i> N <i><sub>x</sub></i> Visible Photocatalyst Prepared by N-Doping in Et <sub>3</sub> N/EtOH Fluid under Supercritical Conditions. Journal of Physical Chemistry C, 2008, 112, 6546-6550.	3.1	58
200	Self-Assembly of Mesoporous Rutheniumâ^'Boron Amorphous Alloy Catalysts with Enhanced Activity in Maltose Hydrogenation to Maltitol. Journal of Physical Chemistry C, 2008, 112, 11448-11453.	3.1	20
201	Ordered Mesoporous Ni Nanowires with Enhanced Hydrogenation Activity Prepared by Electroless Plating on Functionalized SBA-15. Chemistry of Materials, 2008, 20, 3936-3943.	6.7	34
202	Water-Medium Barbier Reaction over a Mesoporous Pd(II) Organometallic Catalyst Immobilized on the Ethyl-Bridged PMOs. Journal of Physical Chemistry C, 2008, 112, 6366-6371.	3.1	23
203	Nanocrystalline Fe/TiO <sub>2</sub> Visible Photocatalyst with a Mesoporous Structure Prepared via a Nonhydrolytic Solâ~Gel Route. Journal of Physical Chemistry C, 2007, 111, 18965-18969.	3.1	167
204	Water-medium Ullmann reaction over a highly active and selective Pd/Ph-SBA-15 catalyst. Green Chemistry, 2007, 9, 1223.	9.0	28
205	A green process for O-heterocyclization of cycloocta-1,5-diene by peroxotungstic species with aqueous H2O2. Green Chemistry, 2007, 9, 878.	9.0	9
206	Aqueous medium Ullmann reaction over a novel Pd/Ph–Al-MCM-41 as a new route of clean organic synthesis. Green Chemistry, 2007, 9, 273-280.	9.0	46
207	Water-medium isomerization of homoallylic alcohol over a Ru(ii) organometallic complex immobilized on FDU-12 support. Green Chemistry, 2007, 9, 500.	9.0	41
208	Supercritical Preparation of a Highly Active S-Doped TiO2Photocatalyst for Methylene Blue Mineralization. Environmental Science & amp; Technology, 2007, 41, 4410-4414.	10.0	258
209	Mesoporous Titania Spheres with Tunable Chamber Stucture and Enhanced Photocatalytic Activity. Journal of the American Chemical Society, 2007, 129, 8406-8407.	13.7	1,119
210	Selective maltose hydrogenation to maltitol on a ternary Co–P–B amorphous catalyst and the synergistic effects of alloying B and P. Applied Catalysis A: General, 2007, 325, 34-40.	4.3	90
211	Mesoporous Au/TiO2Nanocomposites with Enhanced Photocatalytic Activity. Journal of the American Chemical Society, 2007, 129, 4538-4539.	13.7	777
212	Highly Active TiO2N Photocatalysts Prepared by Treating TiO2Precursors in NH3/Ethanol Fluid under Supercritical Conditions. Journal of Physical Chemistry B, 2006, 110, 1559-1565.	2.6	257
213	Homoallylic Alcohol Isomerization in Water over an Immobilized Ru(II) Organometallic Catalyst with Mesoporous Structure. Journal of Physical Chemistry B, 2006, 110, 22942-22946.	2.6	59
214	Self-assembly of mesoporous Ni–B amorphous alloy catalysts. Journal of Catalysis, 2006, 244, 251-254.	6.2	105
215	Direct dehydrogenation of methanol to formaldehyde over pre-treated polycrystalline silver catalyst. Catalysis Letters, 2005, 99, 83-87.	2.6	11
216	Liquid phase acetonitrile hydrogenation to ethylamine over a highly active and selective Ni–Co–B amorphous alloy catalyst. Applied Catalysis A: General, 2004, 275, 199-206.	4.3	90

#	Article	IF	CITATIONS
217	Amorphous Ni-B/SiO2 catalyst prepared by microwave heating and its catalytic activityin acrylonitrile hydrogenation. Journal of Chemical Technology and Biotechnology, 2003, 78, 512-517.	3.2	12
218	Several types of oscillations in Belousov-Zhabotinskii reactions with amino acids as organic substrates. International Journal of Chemical Kinetics, 2002, 34, 405-410.	1.6	3
219	Selective hydrogenation of cinnamaldehyde to cinnamyl alcohol over an ultrafine Co-B amorphous alloy catalyst. Applied Catalysis A: General, 2002, 225, 117-130.	4.3	97
220	Glucose hydrogenation over Ni–B/SiO2 amorphous alloy catalyst and the promoting effect of metal dopants. Catalysis Today, 2002, 74, 53-63.	4.4	116
221	Micro-Raman spectroscopy of Pd-B/SiO2 amorphous alloy catalyst. Journal of Raman Spectroscopy, 2000, 31, 1051-1055.	2.5	10
222	Glucose Hydrogenation to Sorbitol over a Skeletal Ni-P Amorphous Alloy Catalyst (Raney Ni-P). Journal of Catalysis, 2000, 191, 257-260.	6.2	107
223	Title is missing!. Catalysis Letters, 1999, 62, 201-207.	2.6	30
224	Belousov-Zhabotinskii type oscillations with amino acids or peptides as organic substrates in the presence of Mn2+ and Fe(phen)32+ as coupled catalysts. International Journal of Chemical Kinetics, 1998, 30, 243-247.	1.6	5
225	Chapter 4. Preparation and catalytic applications of amorphous alloys. Catalysis, 0, , 144-186.	1.0	13